Numerical investigation of the unsteady transition between asymmetric shock systems

Laguarda Sanchez, Luis; Hickel, Stefan; Schrijer, Ferdinand; van Oudheusden, Bas

Publication date
2019

Document Version
Accepted author manuscript

Published in
54th 3AF International Conference AERO2019 At: Paris, France

Association Aéronautique et Astronautique de France

54th 3AF International Conference on Applied Aerodynamics
25 — 27 March 2019, Paris – France

FP42-AERO2019-laguardasanchez

NUMERICAL INVESTIGATION OF THE UNSTEADY TRANSITION BETWEEN ASYMMETRIC SHOCK SYSTEMS

L. Laguarda, S. Hickel, F. F. J. Schrijer and B. W. van Oudheusden
Faculty of Aerospace Engineering, Technische Universiteit Delft
Kluyverweg 1, 2629HS Delft (The Netherlands), l.laguardasanchez@tudelft.nl

ABSTRACT

The dynamic interaction of two planar and asymmetric shock waves at a free-stream Mach number $M_\infty = 3$ is studied numerically in order to characterize the transition between the regular (RI) and Mach (MI) interaction patterns. Shock deflection disturbances are independently introduced in the form of a sinusoidal oscillation of the shock generator. Selected amplitudes of oscillations ensure that both boundaries of the theoretical dual solution domain (DSD) are crossed every period. The range of angular frequencies investigated resembles the dynamics of the separation shock in shock-wave/turbulent boundary-layer interactions. Computational results show that the MI unambiguously prevails regardless of the initial wave pattern disturbed, provided that the oscillation frequency is not too large. This holds for mean conditions embedded inside the DSD. For those outside, a RI⇄MI alternation is observed when the initial wave pattern is a RI, and no single event of a RI interaction occurs when the initial patter is a MI.

1. INTRODUCTION

Practically relevant high speed aerodynamics applications such as supersonic intakes and nozzle flows, often involve the presence of highly asymmetric shock wave structures. It is well known that for a range of parameters, these shock structures form a bi-stable system for which either the regular interaction (RI) and the Mach interaction (MI) wave patterns materialize. The former, depicted in Figure 1a, involves five discontinuities: two incident C_1,C_2 and two reflected C_3,C_4 shock waves, and one slipline s. They all intersect at one location. Alternatively, the MI includes a fifth quasi-normal shock wave, the Mach stem m, which segregates shock waves C_1 and C_3 from C_2 and C_4. As a result, two sliplines s_1 and s_2 emerge instead of one, see Figure 1b.

Classical gas dynamics theory characterizes stationary shock interactions [1]. Compatibility conditions for the RI require equal static pressure and flow deflection across the slipline s. The latter condition, if flow deflections are taken positive counter-clockwise, implies that

$$\vartheta_1 - \vartheta_3 = \vartheta_2 - \vartheta_4 \tag{1}$$

Given a certain free-stream Mach number M_∞, the aforementioned relation can only be satisfied for a subset of values in the ϑ_1-ϑ_2 space. Considering all possible combinations, a stability boundary called the *detachment* criterion can be drawn in the ϑ_1-ϑ_2 plane. For $M_\infty = 3$, it corresponds to the solid line in Figure 1c which divides the domain in two regions, one where a stationary RI is possible (below) and one where it is impossible (above).

For the MI configuration, the compatibility condition arises from the fact that the pair of sliplines s_1-s_2 should form a convergent duct in order to allow the subsonic flow after the Mach stem m to accelerate. In the presence of one or more Prandtl–Meyer expansions (PME), an extra divergent side of the duct is generated allowing the flow to reach sonic conditions at the throat and further accelerate to supersonic velocities. The height of the resulting Mach stem m for a stationary wave system is such that a suitable duct inlet-to-throat ratio is attained. Static pressure remains constant across both sliplines, but pressure varies inside the subsonic duct which results in a curved Mach stem m. In terms of flow deflections, the requirement for convergent sliplines implies that

$$\vartheta_3 - \vartheta_1 > \vartheta_2 - \vartheta_4 \tag{2}$$

The limit case thus corresponds to the conditions for which s_1 and s_2 are no longer convergent but parallel,

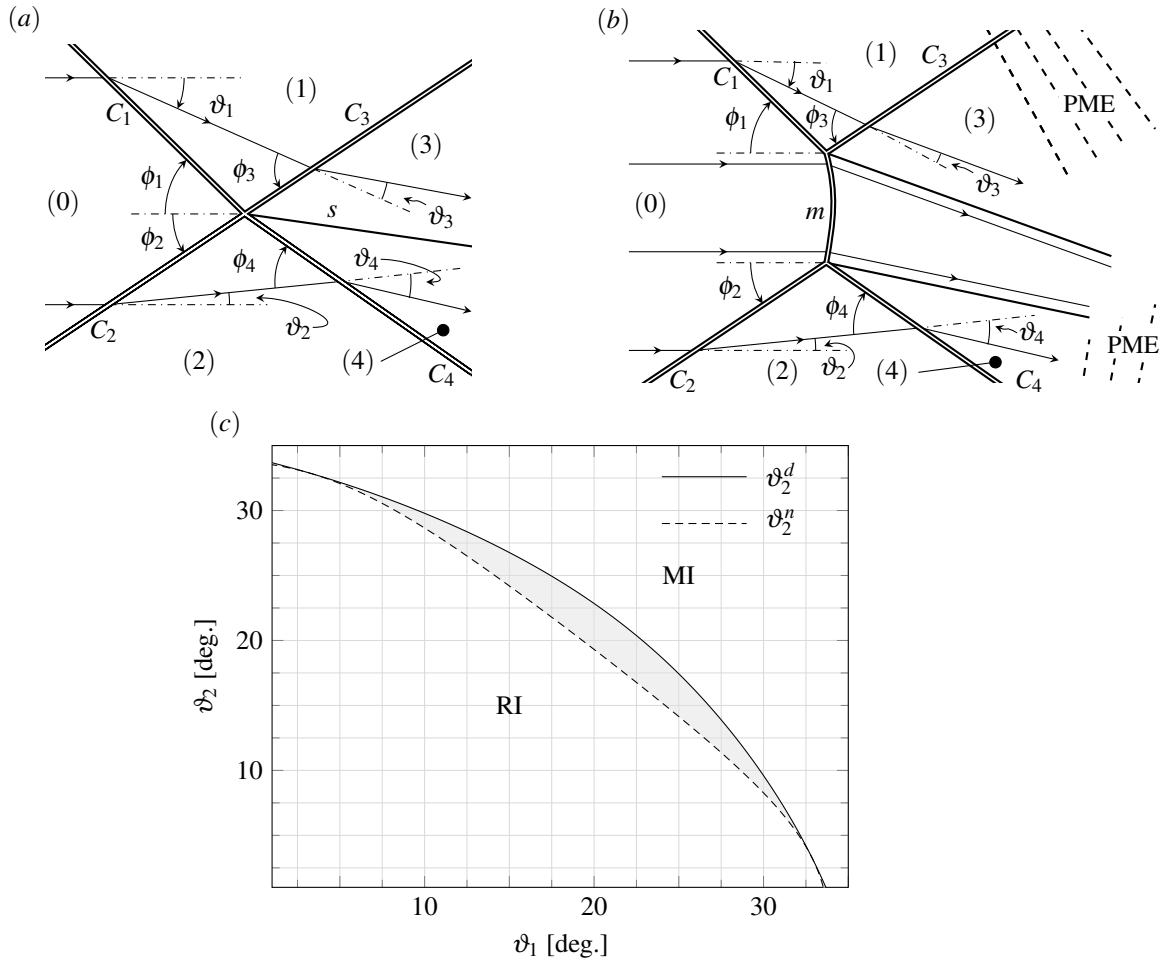

Figure 1: (a) Schematic of a regular interaction pattern with asymmetric incident shock waves, (b) schematic of a Mach interaction pattern with asymmetric incident shock waves, and (c) dual solution domain (shaded in gray) in the ϑ_1-ϑ_2 space at a free-stream Mach number $M_\infty = 3$. The dashed line indicates the *von Neumann* condition and the solid line the *detachment* criterion.

for which eq. 2 reduces to eq. 1. This defines the stability boundary of the MI, and it is called the *mechanical equilibrium* criterion since the pressure jump through the shock system is the same as for the corresponding RI for the same flow deflections. Considering all possible combinations in the ϑ_1-ϑ_2 space satisfying the aforementioned, the dashed line in Figure 1c is defined. It also segregates the domain in two regions: one where the MI is physical (above) and one where it is unstable (below). Many works on the topic often refer to this boundary as the *von Neumann* condition in honor of the author of [14]. It is worth mentioning that useful intuition behind the *von Neumann* and *detachment* conditions is usually provided through a shock polar analysis. It is based on a graphical representation of the Rankine-Hugoniot relations across C_1, C_2, C_3 and C_4 in the pressure-deflection plane where the compatibility conditions are defined. For a detail explanation of the method the reader is referred to [11] and [1].

It is clear from Figure 1c that the *von Neumann* and *detachment* conditions are distinct and enclose a range of flow deflections where both the RI and the MI are physically possible. This region is called the *dual-solution domain* (DSD) [5]. Under the framework of stationary and symmetric shock interactions, Hornung *et al.* [5] put forward the hypothesis that a characteristic flow hysteresis should manifest when the DSD is smoothly penetrated either from the RI or the MI domain. On these grounds, they advocated that RI→MI transition should occur at the *detachment* criterion and the MI→RI transition at the *von Neumann* condition. Numerous experimental studies, e.g. [6] and [3] among others, were conducted thereafter on a symmetric wedge set-up in order to validate the ideas put forward by Hornung *et al.* [5], but in general no DSD was revealed - transition was occurring close to the *von Neumann* condition regardless of the initial wave pattern. Discrepancies between theoretical predictions and experimental data raised the popularity of the problem and in-

centivized numerical investigations on the topic. Computations reported in [7] and [2] did succeed at revealing the predicted hysteresis and the width of the theoretical DSD. It was soon after concluded by [8] and [10] that the presence of free-stream disturbances in the flow were capable of promoting RI→MI transition.

Therefore, it becomes clear that the transition between shock structures in real life applications is a complex dynamic phenomenon. Up to date, very few publications have tackled the problem of dynamic shock interactions in a systematic manner. Kudryavtsev *et al.* [10] and Khotyanovsky *et al.* [9] considered the effects of isolated free-stream disturbances either in the form of an elementary wave (shocks, expansion waves and contact discontinuities) or a laser pulse. Their results indicate that the MI type is the most robust wave pattern inside the DSD because the temporal and spatial scale of the disturbances required to trigger transition to RI is larger than in the opposite case. However, only the effect of isolated disturbances on a symmetric wave system was examined, whereas multiple aerospace applications involving shock interactions evidence that asymmetric rather than symmetric wave systems are more prompt to occur. If one considers a very relevant scenario in supersonic flight, the shock-wave/turbulent boundary-layer interaction (SWTBLI) with mean boundary-layer separation, a characteristic unsteadiness of the separation shock with varying flow deflection is observed. This constant excitation of the shock system may play a role on the character of the shock interaction materializing outside of the turbulent boundary-layer (TBL), which for this type of flows is highly asymmetric. Large-eddy simulations (LES) performed by Matheis and Hickel [12] on a SWTBLI at $M_\infty = 2$ demonstrates that the transient nature of the flow deflection across the separation shock suffices not only to trigger premature RI⇄MI transition, but also to sustain the MI over a long integration time for mean flow deflections in the RI domain where the MI is unstable. Their computations at $M_\infty = 3$ also revealed premature RI⇄MI transition for mean flow deflections embedded within the theoretical DSD. Such an unbalanced excitation of an asymmetric shock system has not been captured in previous investigations on dynamic shock interaction and thus, due to their relevance in high speed flight, demands a more fundamental study.

In the present paper, we thus conduct a numerical investigation to provide insight on the inviscid transition dynamics between asymmetric interactions of planar shock waves triggered by periodic excitations. Two wedges are used to asymmetrically deflect the free-stream flow at $M_\infty = 3$ and introduce the incident shock waves and the PME's in the computational domain. In order to resemble the characteristic unsteadiness of the separation shock in SWTBLI, a sinusoidal oscillation of the lower wedge deflection around a nominal value is imposed with sufficiently large amplitudes to enforce transition and characteristic oscillation frequencies of TBL's.

This paper is organized as follows. In §2 we describe our numerical method and the setup. Three different cases are considered for the computations of periodic excitations: A) the initial flow deflections ϑ_1 and ϑ_2 across the incident shocks are embedded within the theoretical DSD (see Figure 1c), B) the flow deflections are located outside of DSD on the RI side, and C) the flow deflections are located outside the DSD on the MI side. Numerical results are discussed in §3.1 for case A and in §3.2 for cases B and C. Conclusions and further remarks are given in §4.

2. COMPUTATIONAL SETUP

We solve the two-dimensional unsteady Euler equations in differential conservative form

$$\frac{\partial \mathbf{U}}{\partial t} + \frac{\partial \mathbf{F}}{\partial x} + \frac{\partial \mathbf{G}}{\partial y} = 0 \tag{3}$$

where

$$\mathbf{U} = \begin{bmatrix} \rho \\ \rho u \\ \rho v \\ E \end{bmatrix}, \mathbf{F} = \begin{bmatrix} \rho u \\ \rho u^2 + p \\ \rho uv \\ u(E+p) \end{bmatrix}, \mathbf{G} = \begin{bmatrix} \rho v \\ \rho uv \\ \rho v^2 + p \\ v(E+p) \end{bmatrix} \tag{4}$$

The above equations are non-dimensionalized using the free-stream velocity u_∞ and the wedge hypotenuse w, which combined define the characteristic time scale w/u_∞ of the problem. To close the system, the equation of state for perfect gases is used

$$p = (\gamma - 1)\left(E - \rho \frac{u^2 + v^2}{2}\right) \tag{5}$$

with the specific heats ratio $\gamma = 1.4$.

The system of governing equations is discretized on a Cartesian grid with a conservative finite volume scheme. The in-house solver INCA has been used for the computations. Fluxes are obtained as follows: first they are computed using the Roe average of the primitive variables at the cell faces, then they are projected into the right eigenvector space where a global Lax-Friedrichs flux vector splitting and a third-order WENO reconstruction is performed [13], and finally they are projected back to the conserved quantities. A third-order explicit Runge-Kutta scheme is used for time integration [4].

A sketch of the computational domain is included in Figure 2. We consider two wedges of hypotenuse w asymmetrically deflecting the free-stream flow at $M_\infty = 3$ and generating a pair of intersecting waves C_1, C_2 and centered PME's around their trailing edge. The wedges are not included in the computational domain, however. Instead, we account for their effect through time

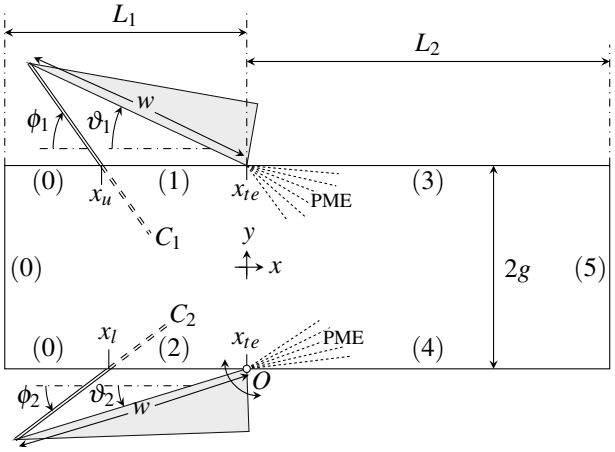

Figure 2: Computational domain and definition of relevant parameters.

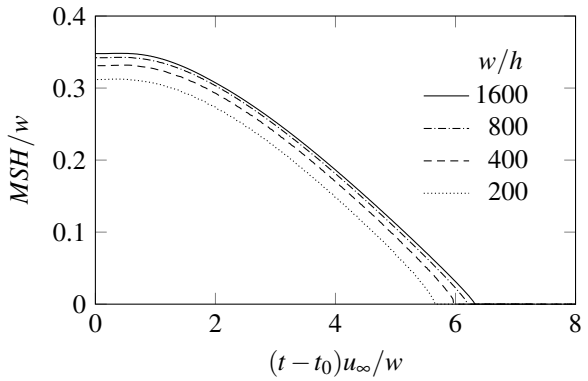

Figure 3: Corresponding Mach stem height evolution for $d\vartheta_2(t)/dt = 0.01w/u_\infty$ rad s^{-1} and different grid sizes $h = \Delta x = \Delta y$.

dependent boundary conditions satisfying the Rankine-Hugoniot relations for the incident shocks $\{(0)\rightarrow(1), (0)\rightarrow(2)\}$ and the Prandtl-Meyer relations for the centered PME's $\{(3), (4)\}$. The upstream extension of the domain L_1 from the stream-wise location of the trailing edges is such that the inlet conditions at the left boundary correspond to the free-stream (0) at all time instances. Similarly, L_2 ensures that the flow at the outlet (5) is always supersonic. The characteristic length scale of the geometry is imposed through the ratio $2g/w$, which is set to 0.84.

The problem is discretized on a uniform grid with spacing h in both spatial directions. A grid convergence analysis is performed to asses the impact of the shock thickness on the Mach stem height (MSH) evolution and the transition process. The MSH is considered as the vertical distance between both ends of m in Figure 1b. An initially steady MI with $\vartheta_1 = 25^\circ$ and $\vartheta_2 = 19^\circ$ (outside of DSD, see Figure 1c) is obtained for an integration time of more than 50 flow through times (FTT). Transition to RI is then enforced by decreasing the lower wedge deflection at a constant angular speed $d\vartheta_2(t)/dt = 0.01u_\infty/w$. The MSH evolution with respect to the flow deflection measured at a distance $0.01w$ below the C_2-C_4 intersection is investigated for four different grid spacings: $w/h = 200, 400, 800$ and 1600. Results are shown in Figure 3 for sampling intervals of $0.025w/u_\infty$ in all cases. A clear convergence is observed for $w/h = 1600$ and thus is used for all computations hereafter.

Simulations with a periodic excitation of the shock system are initialized with a steady state solution, then perturbed asymmetrically by a sinusoidal oscillation of the lower wedge deflection $\vartheta_2(t)$:

$$\vartheta_2(t) = \vartheta_2^i + \Delta\vartheta \sin(2\pi f(t-t_0) + \phi), \qquad (6)$$

where ϑ_2^i, $\Delta\vartheta$, f, t_0 and ϕ correspond to the mean lower wedge deflection, the amplitude of oscillation, the frequency of oscillation, the time at which the oscillatory motion is initiated and the phase shift respectively. Regarding the initial steady state solution, three different cases are considered:

A) the corresponding ϑ_1-ϑ_2 combination is located exactly in the middle of the DSD,

B) the ϑ_1-ϑ_2 combination is located outside of the DSD on the RI side,

C) the ϑ_1-ϑ_2 combination is located outside of the DSD on the MI side.

The upper wedge deflection ϑ_1 is kept at 25° in all computations, and ϑ_2 is set as 15.78°, 13.89° and 17.66° for cases A, B and C respectively. A close-up view of the region of interest of the DSD in the ϑ_1-ϑ_2 space is shown in Figure 4 where all cases are highlighted. For case A, both the initial RI and MI are investigated. In order to obtain the steady solution for the latter, the lower flow deflection of the steady wave pattern in case C is slowly decreased from 17.66° to 15.78° and then kept unaltered until the MSH remains constant over time.

The oscillatory motion of the lower shock generator commences at $t = t_0$ and its initial effect is to bring $\vartheta_2(t)$ closer to the stability limit of the initial steady wave pattern. This implies that $\vartheta_2(t)$ initially increases if the starting wave pattern is a RI, and decreases if it is a MI. Thus, a phase shift of $\phi = 180^\circ$ is required in equation 6 for the latter. Concerning the amplitudes of oscillation $\Delta\vartheta$ in eq. 6, they are chosen according to the theoretical extent of the DSD. For case A, Figure 4 shows that an amplitude of 2° suffices to bring $\vartheta_2(t)$ outside of the DSD in both directions. For case B and C, a larger amplitude of 4° is used. The theoretical *von Neumann* and *detachment* conditions for $M_\infty = 3$ and $\vartheta_1 = 25^\circ$ correspond to $\vartheta_2^v = 14.14^\circ$ and $\vartheta_2^d = 17.43^\circ$ respectively.

The frequency of oscillation is the last parameter required to close the problem. It is well established for

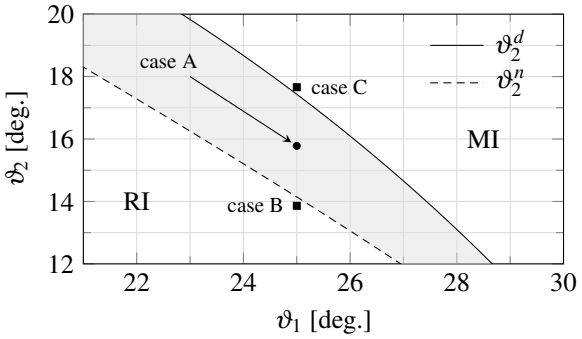

Figure 4: Close-up view of the theoretical DSD (shaded in gray) around the cases considered. The dashed line indicates the *von Neumann* condition and the solid line the *detachment* criterion.

SWTBLI that, even though a broad range of temporal frequencies are involved, those related to the motion of the separation shock are typically about two orders of magnitude lower than u_∞/δ, being δ the 99% incoming boundary-layer thickness. On these lines, an excitation frequency of $f_1 = 0.125u_\infty/w$ appears to be in good agreement with the literature, specially with [12] in which a explicit relation between δ and w is imposed. In order to assess the effect of increasing excitation frequency f in the response of the wave system, frequencies $f_2 = 0.25u_\infty/w$ and $f_3 = 0.5u_\infty/w$ are additionally considered.

3. RESULTS

3.1 Wave pattern inside DSD (case A)

The periodic excitation of an initially steady RI and MI were simulated independently. Numerical data corresponding to an oscillation frequency of $f_1 = 0.125u_\infty/w$ reveals that RI→MI transition occurs during the first period of oscillation when the initial wave pattern is a RI, and thereafter the MI configuration unambiguously prevails. However, this does not hold for larger excitation frequencies $f_2 = 0.25u_\infty/w$ and $f_3 = 0.5u_\infty/w$ where a constant RI⇄MI alternation is observed at every period. Regarding the excitation of an initial MI configuration, transition to RI never takes place for any of the frequencies investigated.

Consider Figures 5a-c where the evolution of the MSH, the instantaneous lower flow deflection $\vartheta_2(t)$ below the intersection C_2-C_4, and the instantaneous flow pressure downstream of intersections C_1-C_3 (blue line) and C_2-C_4 (orange line) for the excitation frequency $f_1 = 0.125u_\infty/w$ are included. Solid lines describe the case of an initial RI pattern, and dashed lines denote the case of an initial MI. For the former, even though both stability boundaries (dashed blue lines in Figure 5b) are crossed during every period, the Mach stem appears the first time the *detachment* condition is exceeded and never disappears again. During this single RI→MI transition event, a characteristic discontinuity in pressure is observed. This discontinuity, which propagates downstream in the form of a pressure wave, appears because the pressure jump through the shock system is different for the RI and the MI at *detachment*. A sequence of instantaneous impressions of the density gradient magnitude for four different time instances in the first period of oscillation is shown in Figures 6a-d. For the sake of completeness, red squares corresponding to the instantaneous MSH, $\vartheta_2(t)$ and pressure of the flow impressions are introduced in Figures 5a-c respectively. The precise instant of transition is captured in Figure 6a. Notice how a kink in both reflected shocks is generated as the pressure wave travels downstream. For the upper reflected shock C_3, the pressure wave segregates the strong shock solution characteristic of the RI at *detachment* (where the flow is subsonic, embedded within the yellow line defining the sonic contour $M = 1$) from the post-wave state corresponding to the weak shock solution associated to the emerging MI.

The relative orientation of the sliplines in Figure 6a is key for preventing any further transition back to RI. As the MI configuration emerges from the interaction, the resulting pair of sliplines emanating from each end of the Mach stem m form a convergent duct within which the subsonic flow accelerates. However, since both sliplines intersect before being influenced by the PME's, the subsonic flow momentarily chokes. This results in an over-pressure that pushes the Mach stem upstream and forces it to grow. Notice the clear difference between the MSH in Figures 6a and b. In Figure 6b, the sliplines have reached the domain of influence of the PME's already, but at this time instance the lower flow deflection $\vartheta_2(t)$ at the interaction has been reduced to a magnitude below the *von Neumann* condition, which makes the MI unstable. The relative orientation of the sliplines, as observed in the figure is thus divergent, which promotes the reduction of the Mach stem size to that of Figure 6c. If the shock system was exposed to such boundary conditions for a sufficiently long period of time, MI→RI transition would eventually happen. Nevertheless, due to the oscillating behavior of the lower wedge, this is not the case. The imposed increase of $\vartheta_2(t)$ again results into a convergent slipline configuration in which the subsonic flow accelerates. Even though the sliplines are already embedded inside the domain of influence of the PME's, the current inlet-to-throat ratio between the MSH and the minimum slipline distance is not suitable for a steady configuration. This prevents the flow going through m to be swallowed at sonic conditions at the throat, which is again translated into choking, an over-pressure inside the duct and a consequent growth of the MSH (see Figure 6d). The process is then periodically repeated and the MSH converges to an oscillation steady mean value as observed in Figure

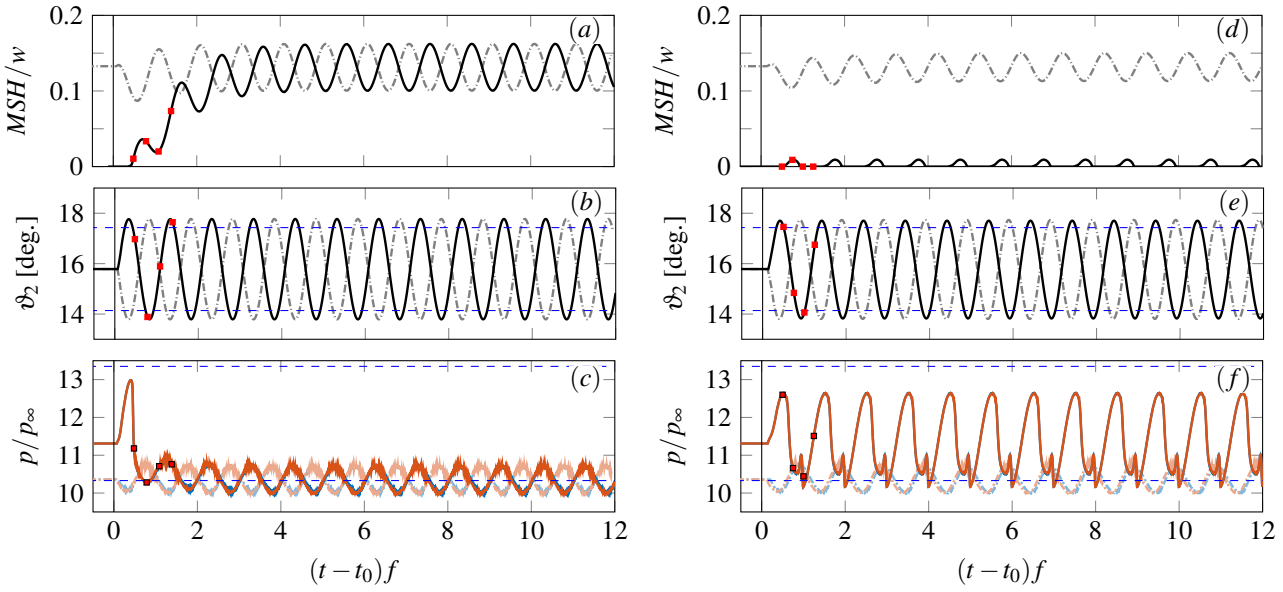

Figure 5: Numerical data for case A with an initial RI under an excitation frequency of: (a)-(c) $f_1 = 0.125u_\infty/w$, and (d)-(e) $f_2 = 0.25u_\infty/w$. The start time of oscillation is denoted by t_0, and the time axis is non-dimentionalized with the excitation frequency f. MSH is the Mach stem height measured as the vertical distance between the extremes of m in figure 1b. ϑ_2 corresponds to the flow deflection measured below the C_2-C_4 intersection at a distance $0.01w$. p/p_∞ is the pressure ratio measured at a distance $0.01w$ downstream of the C_1-C_3 intersection (blue) and C_2-C_4 intersection (orange). Dashed horizontal blue lines highlight the values at *detachment* (upper) and *von Neumann* (lower) conditions.

5a. It is important to note that the evolution of the MSH and pressure behind m after several periods of oscillation is independent of the initial steady state solution (compare solid and dashed lines in Figures 5a and c).

Results for the other frequencies considered, $f_2 = 0.25u_\infty/w$ and $f_3 = 0.5u_\infty/w$, show that transition to MI still occurs when disturbing an initial RI but the former wave pattern is not sustained thereafter. Instead, a constant alternation between RI and MI is observed. Considering the MSH evolution included in Figure 5d for the excitation frequency f_2, the Mach stem emerges and disappears during every period. The associated pressure signal, shown in Figure 5f, oscillates accordingly between characteristic RI and MI levels. Four snapshots within the first period of oscillation for f_2 are included in Figures 6e-h where the density gradient magnitude is shown. The exact times correspond to the red squares highlighted in Figures 5d-f. Starting from Figure 6e, the flow deflection $\vartheta_2(t)$ at this point is above the *detachment* condition, which makes the RI unstable. Thus, a two slipline configuration can already be identified. Additionally, the strong shock solution for some portion of C_3 and C_4 is still materializing. However, moving from Figure 6e to f reveals very important features that are key to explain why the MI is not sustained. The MSH associated to Figure 6f coincides in magnitude with that for Figure 6d. Yet, if one compares both figures, it can be seen that the strong shock solution for the wave C_3 is still present in the latter. This indicates that conditions downstream of the traveling pressure wave are those associated to an RI close to *detachment*. Conversely, the strong shock solution for C_3 has totally vanished in Figure 6f. This is because the flow deflection $\vartheta_2(t)$ below the C_2-C_4 intersection has changed already to a value close to the *von Neumann* condition. The resulting pair of sliplines thus becomes divergent and forces the Mach stem to reduce its size and eventually collapse at the interaction point. This situation corresponds to figure 6g where another discontinuity in pressure is observed. This one is attributed to the acceleration effect of the Mach stem collapsing at the interaction point, which locally produces a peak in pressure as observed in Figure 5f. This discontinuity travels downstream in the form of another pressure wave (see Figure 6h) and the process is repeated as the oscillation of the lower wedge progresses. Results for the angular frequency $f_3 = 0.5u_\infty/w$ are not shown as they do not reveal further information than those for $f_2 = 0.25u_\infty/w$.

Therefore, results demonstrate that the low frequency motion of the lower incident shock in SWTBLI can trigger RI→MI transition and sustain the MI when the disturbed wave pattern is included inside the theoretical DSD. Our findings are consistent with the computations of Matheis and Hickel [12] for a SWTBLI at $M_\infty = 3$ where they also observed the MI materializing for mean flow deflections embedded within the DSD. Numerical data indicates, however, that excitation frequencies of magnitude $0.25u_\infty/w$ and above prevent the MI from prevailing over an extended integration time. This identifies, for the amplitude of oscillation considered ($\Delta\vartheta = 2^\circ$), a certain time scale required for the Mach stem growth

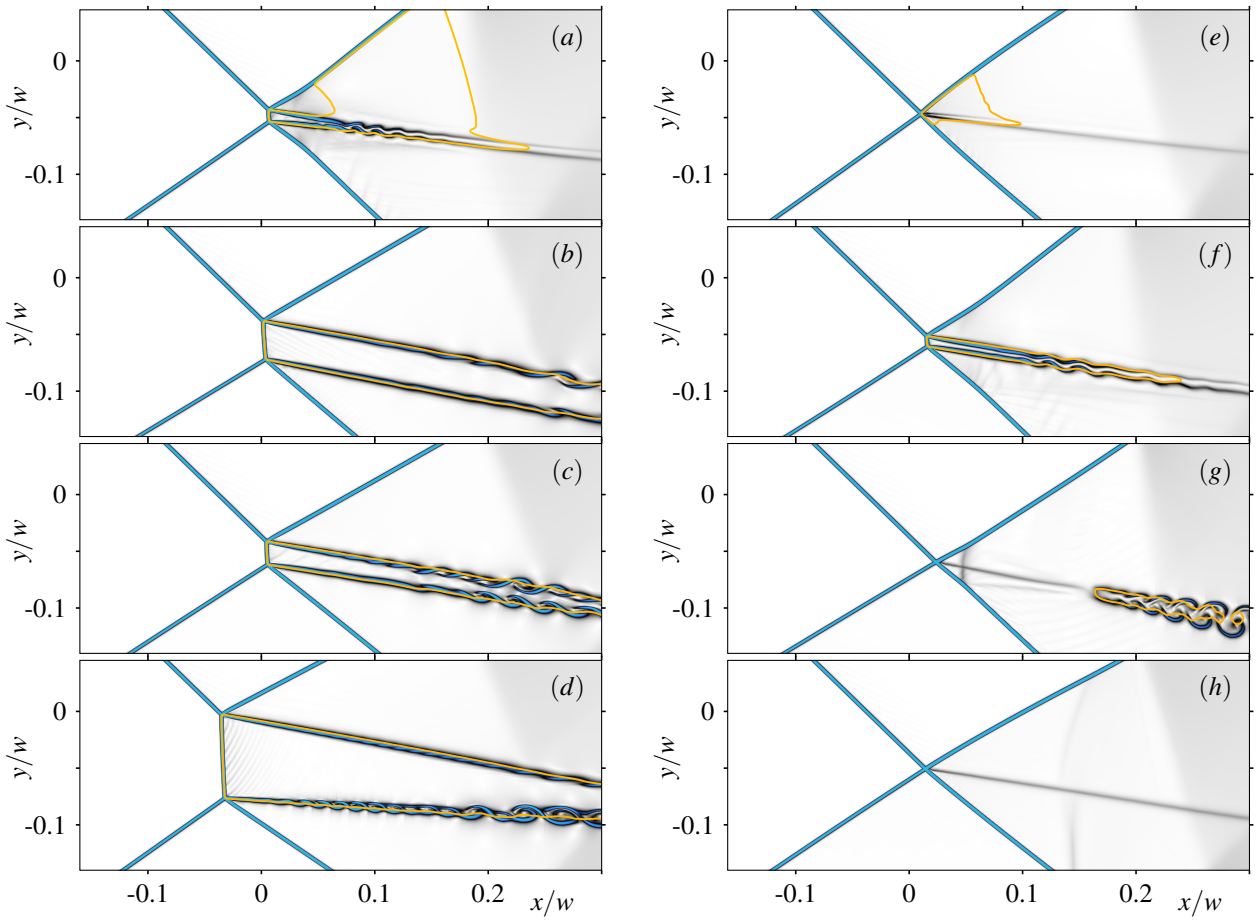

Figure 6: Sequence of instantaneous density gradient magnitude for case A with an initial RI under an excitation frequency of: (a)-(d) $f_1 = 0.125u_\infty/w$, and (e)-(h) $f_2 = 0.25u_\infty/w$. Time instances are marked sequentially as red squares in Figures $5(a)$-(c) and (d)-(f) respectively for f_1 and f_2. The solid yellow line denotes the sonic condition $M = 1$.

and defines a threshold in the frequency of incoming disturbances associated to a TBL that could trigger premature RI→MI in real life experiments. In view of the fact that the MI always materializes when an initial RI is perturbed, whereas for the opposite case the RI configuration never appears, it is then certain to conclude that the MI pattern inside the DSD is more robust in front of perturbations. Also in line with the concluding remarks of Kudryavtsev *et al.* [10] and Khotyanovsky *et al.* [9], larger disturbances are required to enforce MI→RI transition than in the opposite direction.

3.2 Wave pattern outside DSD (cases B&C)

Computations for cases B and C were conducted with the goal of enforcing transition and sustaining the opposite wave pattern for an initial ϑ_1-ϑ_2 combination residing outside of the a DSD. However, for the range of frequencies considered ($f_1 = 0.125u_\infty/w$, $f_2 = 0.25u_\infty/w$ and $f_3 = 0.5u_\infty/w$), this was not found. As observed in the evolution of the MSH included in Figure 7a for case B, transition to MI still occurs but the MI configuration is not sustained. Instead, a constant RI⇆MI alternation is identified similar to that of case A under an excitation frequency larger than $0.125u_\infty/w$. The explanation resides in the evolution of the effective lower flow deflection measured below the C_2-C_4 intersection and shown in Figure 7b. It can be seen that $\vartheta_2(t)$ persists above the *von Neumann* condition for less than half of a period. Within this time, its value changes almost 8°. Even for the lowest excitation frequency ($f_1 = 0.125u_\infty/w$), $\vartheta_2(t)$ still changes twice as fast as the for the largest excitation frequency investigated in case A. Therefore, the boundary conditions change so rapidly that the Mach stem height cannot grow. Regarding the evolution of the MSH and the lower flow deflection included in Figures 7c-d for case C, not a single event of a RI is revealed for the frequencies considered. Rather, a constant shrink and growth of the Mach stem occurs. This circumstance underlines once more that the time scale associated to a disturbance capable of triggering MI⇄RI transition must be larger than in the opposite direction.

A noteworthy feature in case C is the asymmetric response of the Mach stem height during one period of oscillation of the lower incident shock. This becomes more pronounced as the excitation frequency increases,

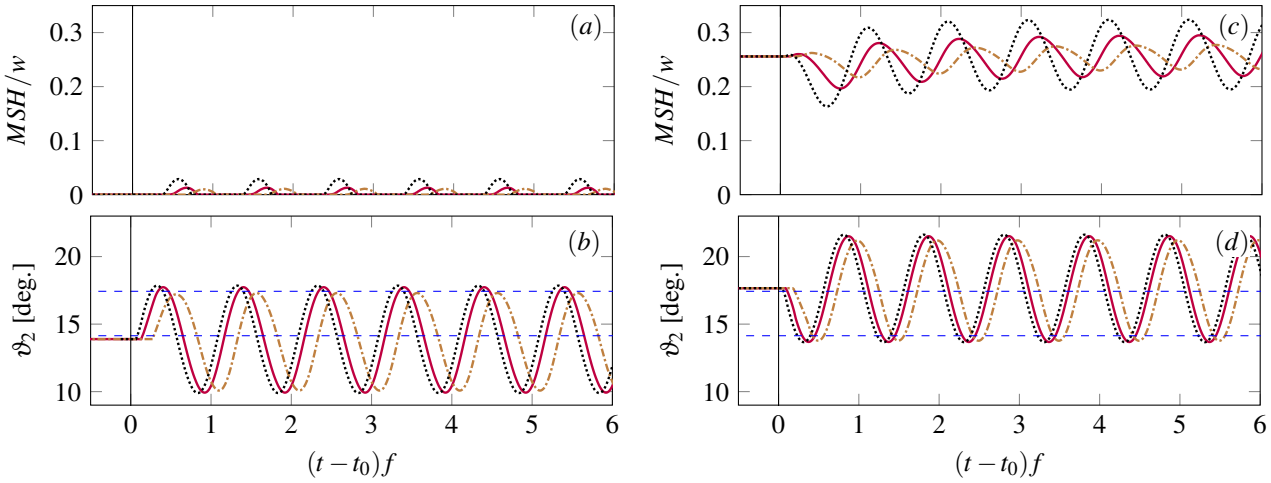

Figure 7: Evolution of the Mach stem height MSH and the lower flow deflection below the C_2-C_4 intersection for the oscillation around $\vartheta_2^i = 13.89°$ (a-b) and $\vartheta_2^i = 17.66°$ (c-d). Dotted lines denote the numerical results for the excitation frequency $f_1 = 0.125u_\infty/w$, solid lines for $f_2 = 0.25u_\infty/w$ and dash-dotted lines for $f_3 = 0.5u_\infty/w$ respectively. The start time of oscillation is t_0, and the time axis is non-dimentionalized with the excitation frequency f. Dashed horizontal blue lines highlight the values at *detachment* (upper) and *von Neumann* (lower) conditions.

see dash-dotted lines in Figure 7c. We believe that this phenomena is associated with a delay in the response of the flow around s_1 essentially because, due to the presence of the Mach stem, it is further away than s_2 from the source of the disturbance (which is the shock foot of C_2 in Figure 2). This delay conditions the speed at which the relative slipline orientation is modified, which in turn influences the Mach stem growth and shrink rate. In Figure 7c it can be seen that the Mach stem grows faster than it shrinks because the upper slipline is modified faster (leading more rapidly to a relative slipline orientation that forces the Mach stem to grow) when the Mach stem is smaller.

In view of the fact that the MI was not sustained (see Figure 7a and b), additional computations were conducted for case B. Instead of an initial RI, the initial steady MI obtained in case C was used as the starting wave pattern. A phase ϕ to the oscillating motion of the lower wedge was then given ($\pi/2 < \phi < \pi$) in order to impose $\vartheta_2(t_0) = 17.66°$. This way, even though the mean value of the lower wedge deflection remained $\vartheta_2^i = 13.89°$ (outside the DSD on the RI domain), the periodic excitation commenced with a fully developed MI. Results for the MSH and the lower flow deflection below the C_2-C_4 intersection are respectively included in Figures 8a and b where it is shown that the MI interaction is still not sustained over time. Instead, what appears to be an exponential decay of the MSH is observed superimposed to the sinusoidal oscillation. Dotted, solid and dash-dotted lines denote excitation frequencies of $f_1 = 0.125u_\infty/w$, $f_2 = 0.25u_\infty/w$ and $f_3 = 0.5u_\infty/w$ respectively, revealing that the aforementioned decay is independent of the excitation frequency. After some periods of oscillation, the evolution of the MSH is identical to that obtained for an initial RI.

Thus, our numerical simulations did not confirm that a MI can be sustained at $M_\infty = 3$ with a periodic excitation of the lower incident shock and mean flow deflections located outside of the DSD on the RI domain. Results indicate that characteristic TBL frequencies together with the amplitudes of oscillation required to traverse the span of the DSD introduce disturbances in the shock system that are too fast for the Mach stem to develop. This is in agreement with the computations of Matheis and Hickel [12] for a SWTBLI at the same free-stream Mach number where also no event of a MI sustained over time was detected for mean flow deflections below the *von Neumann* condition.

4. CONCLUSIONS

Numerical simulations were performed to provide insight on the inviscid transition dynamics between asymmetric interactions of planar shock waves triggered by periodic excitations. Two wedges were used as shock generators at a free-stream Mach number $M_\infty = 3$. Computations were initialized with a steady state solution, either with a RI or a MI, that was then perturbed with a sinusoidal oscillation of the lower wedge deflection around a nominal value. Three different flow deflections for the initial steady wave pattern were considered: A) flow deflections embedded within the DSD, B) flow deflections located outside of the DSD on the RI side, and C) flow deflections located outside on the MI side. Amplitudes of oscillation of 2° for case A and of 4° for cases B and C were chosen based on the theoretical DSD, and the effect of three different excitation frequencies characteristic of

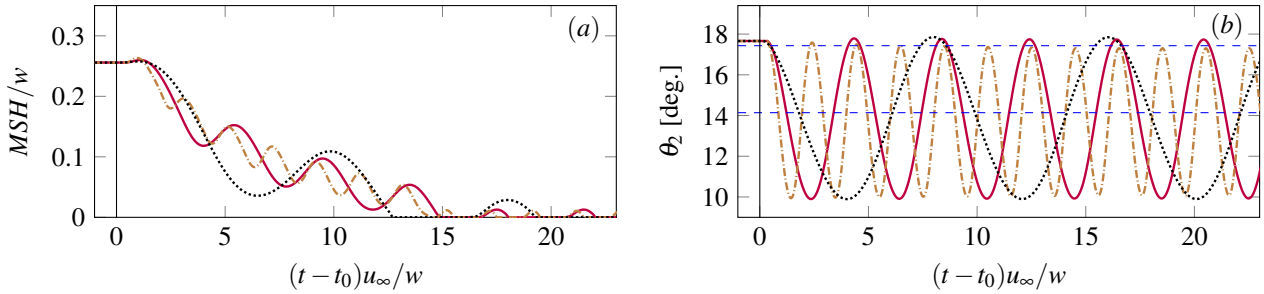

Figure 8: Evolution of (a) the Mach stem height MSH and (b) the lower flow deflection below the C_2-C_4 intersection for the oscillation around $\vartheta_2^i = 13.89°$ with an offset such that $\vartheta_2(t_0) = 17.66°$. The initial steady state solution is that of case C. Dotted lines denote the numerical results for the excitation frequency $f_1 = 0.125u_\infty/w$, solid lines for $f_2 = 0.25u_\infty/w$ and dash-dotted lines for $f_3 = 0.5u_\infty/w$ respectively. The start time of oscillation is t_0, and the time axis is non-dimentionalized with the characteristic time scale w/u_∞. Dashed horizontal blue lines highlight the values at *detachment* (upper) and *von Neumann* (lower) conditions.

TBL's was investigated: $f_1 = 0.125u_\infty/w$, $f_2 = 0.25u_\infty/w$ and $f_3 = 0.5u_\infty/w$.

Results for case A perturbed at an excitation frequency f_1 reveal that the MI unambiguously prevailed regardless of the initial wave pattern. For larger frequencies, however, a constant RI⇆MI was observed. No single event of a RI was detected when the initial wave pattern was a MI. Concerning case B, an amplitude of oscillation of 4° along with the frequencies investigated appeared to introduce flow disturbances in the wave system that were too rapid to allow the Mach stem to grow. Still, a similar RI⇆MI alternation as in case A was found. Oscillations in case C lead to a constant growth and shrink of the Mach stem without the RI materializing. This response of the Mach stem during a period of oscillation is asymmetric (grows faster than it shrinks) and the asymmetry is accentuated with increasing excitation frequency.

In an attempt to sustain the MI for mean flow deflections where it is not stable, the initial steady MI defined in case C was used as the initial wave pattern in case B. A phase was then given to the sinusoidal oscillation of the lower wedge in order to match the flow deflections of both cases at $t = t_0$. This way, a fully developed MI was exposed to the oscillatory motion of the lower incident shock around a mean value below the *von Neumann* condition. For none of the excitation frequencies considered (f_1, f_2 and f_3), however the MI was sustained. Instead, it appeared to decay exponentially with a sinusoidal oscillation superimposed until a constant RI⇆MI alternation was obtained.

Thus, our results demonstrate that a MI can trigger RI→MI transition and sustain the MI for conditions encountered in SWTBLI scenarios with mean flow deflections within the theoretical DSD. This confirms that the MI pattern is the most robust configuration inside the DSD, and that larger disturbances are required to trigger RI→MI transition than in the opposite direction. However, the analysis does not show that the MI can be sustained for mean flow conditions located outside the theoretical DSD on the RI side. This might be attributed to the width of the DSD at $M_\infty = 3$, which extends over several degrees for the upper wedge deflection considered.

REFERENCES

[1] G Ben-Dor. *Shock wave reflection phenomena*, volume 2. Springer, 2007.

[2] A Chpoun and G Ben-Dor. Numerical confirmation of the hysteresis phenomenon in the regular to the mach reflection transition in steady flows. *Shock Waves*, 5(4):199–203, 1995.

[3] A Chpoun, D Passerel, H Li, and G Ben-Dor. Reconsideration of oblique shock wave reflections in steady flows. part 1. experimental investigation. *Journal of Fluid Mechanics*, 301:19–35, 1995.

[4] S Gottlieb and CW Shu. Total variation diminishing runge-kutta schemes. *Mathematics of computation of the American Mathematical Society*, 67(221):73–85, 1998.

[5] HG Hornung, H Oertel, and RJ Sandeman. Transition to mach reflexion of shock waves in steady and pseudosteady flow with and without relaxation. *Journal of Fluid Mechanics*, 90(3):541–560, 1979.

[6] HG Hornung and ML Robinson. Transition from regular to mach reflection of shock waves part 2. the steady-flow criterion. *Journal of Fluid Mechanics*, 123:155–164, 1982.

[7] MS Ivanov, SF Gimelshein, and AE Beylich. Hysteresis effect in stationary reflection of shock waves. *Physics of Fluids*, 7(4):685–687, 1995.

[8] MS Ivanov, GP Klemenkov, AN Kudryavtsev, SB Nikiforov, AA Pavlov, VM Fomin,

AM Kharitonov, DV Khotyanovsky, and HG Hornung. Experimental and numerical study of the transition between regular and mach reflections of shock waves in steady flows. In *The 21st International Symposium on Shock Waves*, 1997.

[9] DV Khotyanovsky, AN Kudryavtsev, and MS Ivanov. Effects of a single-pulse energy deposition on steady shock wave reflection. *Shock Waves*, 15(5):353–362, 2006.

[10] AN Kudryavtsev, DV Khotyanovsky, MS Ivanov, A Hadjadj, and D Vandromme. Numerical investigations of transition between regular and mach reflections caused by free-stream disturbances. *Shock Waves*, 12(2):157–165, 2002.

[11] H. Li, A. Chpoun, and G. Ben-Dor. Analytical and experimental investigations of the reflection of asymmetric shock waves in steady flows. *Journal of Fluid Mechanics*, 390:25–43, 1999.

[12] J Matheis and S Hickel. On the transition between regular and irregular shock patterns of shock-wave/boundary-layer interactions. *Journal of Fluid Mechanics*, 776:200–234, 2015.

[13] CW Shu. Essentially non-oscillatory and weighted essentially non-oscillatory schemes for hyperbolic conservation laws. In *Advanced numerical approximation of nonlinear hyperbolic equations*, pages 325–432. Springer, 1998.

[14] J von Neumann. Oblique reflection of shocks. *Bureau of Ordinance, Explosives Research Report*, 1943.